Theoretical study on rotational bands and shape coexistence of ^{183,185,187}Tl in the particle-triaxial-rotor model

Guo-jie Chen,[1,*] Yu-xin Liu,[2,3,4,†] Hui-chao Song,[5] and Hui Cao[1]
[1]*School of Science, Foshan University, Foshan 528000, China*
[2]*Department of Physics, Peking University, Beijing 100871, China*
[3]*Key Laboratory of Heavy Ion Physics, Ministry of Education, Beijing 100871, China*
[4]*Center of Theoretical Nuclear Physics, National Laboratory of Heavy Ion Accelerator, Lanzhou 730000, China*
[5]*Department of Physics, Ohio State University, Columbus, Ohio 43210, USA*
(Received 5 February 2005; revised manuscript received 15 July 2005; published 9 March 2006)

By taking the particle-triaxial-rotor model with variable moment of inertia, we systematically investigate the energy spectra, deformations, and single-particle configurations of the nuclei ^{183,185,187}Tl. The calculated energy spectra agree quite well with experimental data. The obtained results indicate that the rotation-aligned bands observed in ^{183,185,187}Tl originate from one of the $[530]\frac{1}{2}^-$, $[532]\frac{3}{2}^-$, $[660]\frac{1}{2}^+$ proton configurations coupled to a prolate deformed core. Furthermore, the negative parity bands built upon the $\frac{9}{2}^-$ isomeric states in ^{183,185,187}Tl are formed by a proton with the $[505]\frac{9}{2}^-$ configuration coupled to a core with triaxial oblate deformation, and the positive parity band on the $\frac{13}{2}^+$ isomeric state in ^{187}Tl is generated by a proton with configuration $[606]\frac{13}{2}^+$ coupled to a triaxial oblate core.

DOI: 10.1103/PhysRevC.73.034304 PACS number(s): 21.10.Re, 21.60.Ev, 21.10.Pc, 27.70.+q

I. INTRODUCTION

It has been known that nuclei in the $Z = 82$ region are rich in shape coexistence. In particular, the important deformation-driving orbitals have been assigned as the $h_{9/2}$ and $i_{13/2}$ proton shells [1,2]. In odd-mass Tl isotopes (with $Z = 81$), one-particle-two-hole (1p-2h) intruder states and shape coexistence have been discovered through the observation of low-lying $9/2^-$ isomeric states [3]. The structure of these isomeric states was confirmed as being decided by the odd proton occupying the $h_{9/2}$ intruder orbital [4,5]. Later, the rotational bands associated with both oblate ($\pi h_{9/2}, \pi i_{13/2}$) and prolate ($\pi h_{9/2}, \pi i_{13/2}, \pi f_{7/2}$) structures were observed in lighter isotopes ^{185,187}Tl [6]. The bandhead of the 1p-2h oblate $\pi h_{9/2}$ intruder band has been observed to lie lowest in energy near $N = 108$. In contrast, the bandhead of the prolate intruder band based on the $i_{13/2}$ structure has been predicted to decrease continuously in excitation energy as the neutron number decreases beyond the neutron mid-shell. This prolate structure is presumably formed by coupling the odd $i_{13/2}$ proton to the prolate Hg core with 4p-6h structure [6]. Recently, a rotationallike yrast cascade was established in ^{183}Tl and assigned to associate with the prolate $i_{13/2}$ structure [7]. Furthermore the bandhead energy of its yrast band was later determined [8].

Besides the coexistence of prolate and oblate shapes mentioned above, the signature splitting observed in the $[505]9/2^-$ band in ^{187}Tl, which is significantly larger than that observed in its heavier odd-mass isotopes with $A \geqslant 191$, suggests that there may exist triaxial deformation [1,6]. Moreover, the discrepancy between the calculated equilibrium energy and the experimental data of the bandhead energy of the $[606]\frac{13}{2}^+$ band in ^{187}Tl hints that triaxial deformation may also be involved [6]. However, no concrete investigation on the triaxiality in ^{185,187}Tl has been reported up to now. Furthermore, there does not exist, at present, a systematic theoretical investigation on the structure of ^{183}Tl. In addition, whether the $[532]\frac{3}{2}^-$ ($h_{9/2}$) state in ^{185,187}Tl can be distinguished from the $[530]\frac{1}{2}^-$ ($f_{7/2}$) state (the band formed by such a configuration has not yet been observed in ^{185}Tl) has not yet been determined definitely [6].

On the theoretical side, it is well established that the total energy surface calculation is quite successful in studying the equilibrium shape of a nucleus and shape coexistence (see, for example, Refs. [9–11]). In addition, the projected shell model [12] and particle-triaxial-rotor model [13–15] are also suitable for studying triaxial deformation and configuration mixing [16,17]. However, the triaxial deformation in the light odd-A Tl isotopes has not yet been studied. Because of its simplicity, we take the particle-triaxial-rotor model with the variable moment of inertia of the core to systematically analyze the structure and deformation of the energy bands in ^{183,185,187}Tl and to identify their microscopic configuration.

The paper is organized as follows. We describe briefly the formalism of the particle-triaxial-rotor model in Sec. II. In Sec. III, we describe our calculation and results. In Sec. IV, we give a summary and brief remarks.

II. PARTICLE-TRIAXIAL-ROTOR MODEL

In the particle-rotor model, the Hamiltonian of an odd-A nucleus is usually written as [13–15]

$$\hat{H} = \hat{H}_{\text{core}} + \hat{H}_{\text{s.p.}} + \hat{H}_{\text{pair}}. \quad (1)$$

*Email address: chengj126@126.com
†Corresponding author, email address: yxliu@pku.edu.cn

In the case of triaxial deformation, the Hamiltonian of the even-even core is given as

$$\hat{H}_{\rm core} = \sum_{i=1}^{3} \frac{\hbar^2 R_i^2}{2\Im_i} = \sum_{i=1}^{3} \frac{\hbar^2 (I_i - j_i)^2}{2\Im_i}, \tag{2}$$

where R, I, and j are the angular momentum of the core, nucleus, and single particle, respectively. The three rotational moments of inertia are assumed to be connected by a relation of hydrodynamic type

$$\Im_\kappa = \frac{4}{3}\Im_0(I)\sin^2\left(\gamma + \frac{2\pi}{3}\kappa\right), \tag{3}$$

with

$$\Im_0(I) = \Im_0\sqrt{1 + bI(I+1)}, \tag{4}$$

being the variable moment of inertia [18] of the core to replace the original constant $\Im_0$ to improve the calculation. In the present calculation, we take $b = 0.013$ as the same as that in Refs. [19–21].

$\hat{H}_{\rm s.p.}$ describes the Hamiltonian of the unpaired single particle. In the triaxial deformed field of the even-even core, $\hat{H}_{\rm s.p.}$ is given by

$$\begin{aligned}\hat{H}_{\rm s.p.} = &-\frac{\hbar^2}{2m}\nabla^2 + \frac{1}{2}m\omega_0^2\left\{1 - 2\beta\left[Y_{20}\cos\gamma\right.\right.\\ &\left.\left. + \frac{1}{\sqrt{2}}(Y_{22} + Y_{2-2})\sin\gamma\right]\right\}\\ &- \kappa\hbar\omega_0\{2\vec{l}\cdot\vec{s} + \mu(l^2 - \langle l_N\rangle^2)\},\end{aligned} \tag{5}$$

where κ and μ are Nilsson parameters, Y_{2q} is the rank-2 spherical harmonic function.

$\hat{H}_{\rm pair}$ is the Hamiltonian to represent the pairing correlation which can be treated in the Bardeen-Cooper-Schrieffer (BCS) formalism.

The single-particle wave function can be expressed as

$$|\nu\rangle = \sum_{Nlj\Omega} C^{(\nu)}_{Nlj\Omega}\,|Nlj\Omega\rangle, \tag{6}$$

where ν is the sequence number of the single-particle orbitals, $|Nlj\Omega\rangle$ represents the corresponding Nilsson state, and $C^{(\nu)}_{Nlj\Omega}$ is the coefficient to identify the configuration mixing. Diagonalizing the single-particle Hamiltonian in the basis $|Nlj\Omega\rangle$, we can obtain the $C^{(\nu)}_{Nlj\Omega}$ and the single-particle eigenvalue ε_ν. The corresponding quasiparticle energy can then be determined by $E_\nu = \sqrt{(\varepsilon_\nu - \lambda)^2 + \Delta^2}$, with λ and Δ being the Fermi energy and the energy gap, respectively.

The total Hamiltonian in Eq. (1) can be diagonalized in the symmetrically strong coupling basis

$$|IKM\nu\rangle = \sqrt{\frac{2I+1}{16\pi^2}}\left[D^I_{MK}\alpha^\dagger_\nu|\tilde{0}\rangle + (-1)^{I-K}D^I_{M-K}\alpha^\dagger_{\bar{\nu}}|\tilde{0}\rangle\right], \tag{7}$$

where α^+_ν is the creation operator of the single nucleon (in the present case, the proton) in the orbital $|\nu\rangle$, and D^I_{MK} is the rotational matrix.

III. CALCULATION AND RESULTS

In the present calculation to investigate the property of ^{183,185,187}Tl, we take the κ and μ in standard values [22], i.e., 0.054, 0.690, respectively, and the pairing gap parameter as $\Delta = 12/\sqrt{A}$. To improve the agreement between calculated results and experimental data, we introduce a Coriolis attenuation factor ξ and take its value as that giving the best agreement between the calculated and experimental energy spectra. We found that when $\xi = 0.95$, the calculated results agree best with the experimental data of ^{183,185,187}Tl. In general principle, in order to describe the nuclear property more accurately and to make better agreement between calculated and experimental data, it is necessary to involve a sufficient number of single-particle orbitals near the Fermi surface in the calculation. So we take 13 orbitals near the Fermi surface to couple with the core for ^{183}Tl, ^{185}Tl, and ^{187}Tl. Practical calculation shows that the Fermi levels of the bands 6 (we denote the band labels here as the same as those for the nucleus ^{187}Tl in Ref. [6], so that similar bands can be compared) of the nuclei lie between the 20th and 21st single-particle orbitals, and the others lie between the 19th and 20th. For the deformation parameters β and γ of ^{185,187}Tl, we take those given in Ref. [6] as the trial initial values to fit. For the deformation parameters of ^{183}Tl, since their values have not been reported, we take the values of its neighbor nucleus ^{185}Tl [6] as the trial initial ones. Then we accomplished a series diagonalization of the total Hamiltonian with various values of β and γ to decrcase the calculation error $\chi^2 = \frac{1}{N}\sum_j (E_j^{\rm cal} - E_j^{\rm exp})^2$ of the spectrum of a band, where N is the number of levels in the band. (In such a process, the bandhead energy is fixed artificially with the definite angular momentum assigned in the experiment. The best fit, in fact, is, focused on the energy separations.) Also, it should be noted that the parameter sector we used in the present work is the same as that used by Nilsson and Ragnarsson [23], where β can be positive or negative and γ varies from 0° to 30°. The best fitted values of β and γ are listed in Tables I, II, and III for the nuclei ^{183}Tl, ^{185}Tl, and ^{187}Tl, respectively. Furthermore, we obtain the total wave functions in terms of the single-particle orbitals which, as mentioned above, are fixed by diagonalizing the single-particle Hamiltonian at each set of deformation parameters (β, γ). The calculated main components of the single-particle orbitals in terms of the Nilsson levels (in the case of best fitted deformation parameters) of the nuclei ^{183}Tl, ^{185}Tl, and ^{187}Tl are also listed in Tables I–III, The resulting energy spectra for the nuclei ^{183,185,187}Tl, as obtained from the best fit, are illustrated in Fig. 1. They show good agreement with the experimental data.

Because the experimentally observed rotational bands in ^{187}Tl are richer and more characteristic than those in ^{183}Tl and ^{185}Tl, we analyze as a typical example, the band structure and configuration in ^{187}Tl in detail. To this end, we list in Table IV the wave functions in terms of the single-particle orbitals of the bands in ^{187}Tl.

From Table IV, we can recognize that band 1 originates primarily from the 22nd single-particle orbital coupling with the prolate even-even ^{186}Hg core. Seen from Table III, the 22nd orbital contains a mixture of $54.9\%|5f_{7/2}\tfrac{1}{2}\rangle$, $23.0\%|5p_{3/2}\tfrac{1}{2}\rangle$,

TABLE I. Deformation parameters and main components of single-particle levels $|\nu\rangle$ near the Fermi surface in terms of the Nilsson levels of bands in ^{183}Tl (initial values of the deformation parameters are taken as those of ^{185}Tl in Ref. [6]).

Band	β		γ(deg)		$\|\nu\rangle$	Wave function in terms of $\|Nlj\Omega\rangle$
	Initial value	Fitted value	Initial value	Fitted value		
					$\|19\rangle$	$0.856\|5h_{11/2}\frac{1}{2}\rangle + 0.425\|5f_{5/2}\frac{1}{2}\rangle - 0.182\|5f_{7/2}\frac{1}{2}\rangle$
					$\|20\rangle$	$0.986\|5h_{9/2}\frac{9}{2}\rangle + 0.103\|5h_{9/2}\frac{5}{2}\rangle$
Band 3	−0.162	−0.168	0	15	$\|21\rangle$	$0.764\|5h_{9/2}\frac{7}{2}\rangle + 0.601\|5f_{7/2}\frac{7}{2}\rangle - 0.169\|5h_{9/2}\frac{3}{2}\rangle$
$([505]\frac{9}{2}^-)$					$\|22\rangle$	$0.819\|5h_{9/2}\frac{5}{2}\rangle + 0.385\|5h_{9/2}\frac{1}{2}\rangle - 0.210\|5f_{5/2}\frac{5}{2}\rangle$
					$\|23\rangle$	$0.733\|5h_{9/2}\frac{3}{2}\rangle + 0.392\|5h_{9/2}\frac{1}{2}\rangle + 0.378\|5h_{9/2}\frac{5}{2}\rangle$
					$\|19\rangle$	$0.995\|4g_{9/2}\frac{7}{2}\rangle$
					$\|20\rangle$	$0.967\|4d_{5/2}\frac{5}{2}\rangle + 0.217\|4g_{7/2}\frac{5}{2}\rangle + 0.130\|4g_{9/2}\frac{5}{2}\rangle$
Band 6	0.267	0.270	0	0	$\|21\rangle$	$0.951\|6i_{13/2}\frac{1}{2}\rangle + 0.545\|6g_{9/2}\frac{1}{2}\rangle$
$([660]\frac{1}{2}^+)$					$\|22\rangle$	$0.945\|6i_{13/2}\frac{3}{2}\rangle + 0.511\|6g_{9/2}\frac{3}{2}\rangle$
					$\|23\rangle$	$0.902\|4d_{3/2}\frac{3}{2}\rangle + 0.251\|4s_{1/2}\frac{1}{2}\rangle + 0.216\|5d_{5/2}\frac{3}{2}\rangle$

and 10.7%$|5h_{9/2}\frac{1}{2}\rangle$ configurations. Since the largest component is $|5f_{7/2}\frac{1}{2}\rangle$, band 1 can be assigned as the one arising mainly from the configuration $[530]\frac{1}{2}^-$ ($\pi f_{7/2}$). Meanwhile, from Table IV, we can see that band 2 consists of a mixture of about 93% 20th and 7% 19th orbitals. Seen from Table III, the 20th orbital contains 84.3% $|5h_{9/2}\frac{3}{2}\rangle$ configuration. Thus, we can infer that band 2 is formed by the $[532]\frac{3}{2}^-$ configuration. Similarly, combining Table IV with Table III, we can recognize that bands 5 and 6 originate mainly from the 23rd and 21st single-particle orbital, respectively; the 21st orbital contains 87.4% $|6i_{13/2}\frac{1}{2}\rangle$ configuration, and the 23rd consists of almost purely the $|6i_{13/2}\frac{13}{2}\rangle$ configuration. Therefore, bands 5 and 6 are based on the configuration $\pi[606]\frac{13}{2}^+$, and $\pi[660]\frac{1}{2}^+$, respectively. The above calculated results of bands 1, 2, 5, and 6 are consistent with the prediction of Ref. [6]. And the configuration assignment of bands 1 and 2 is a corroboration of that in Ref. [6]. Furthermore, the $[530]\frac{1}{2}^-$ ($f_{7/2}$) band involves about 10% $h_{9/2}$ configuration and the $[532]\frac{3}{2}^-$ ($h_{9/2}$) band involves only about 4% $f_{7/2}$ configuration. On the other hand, similar results are obtained for the corresponding bands in ^{183,185}Tl.

In order to investigate the deformation nature of band 3 in ^{183,185,187}Tl, we illustrate at first the calculation error

TABLE II. Same as Table I, but for ^{185}Tl.

Band	β		γ		$\|\nu\rangle$	Wave function in terms of $\|Nlj\Omega\rangle$
	Initial value	Fitted value	Initial value	Fitted value		
					$\|18\rangle$	$0.993\|5h_{11/2}\frac{9}{2}\rangle$
					$\|19\rangle$	$0.872\|5h_{9/2}\frac{1}{2}\rangle - 0.420\|5f_{5/2}\frac{1}{2}\rangle + 0.183\|5f_{7/2}\frac{1}{2}\rangle$
Band 2	0.245	0.247	0	0	$\|20\rangle$	$0.910\|5h_{9/2}\frac{3}{2}\rangle + 0.335\|5f_{5/2}\frac{3}{2}\rangle + 0.195\|5f_{7/2}\frac{3}{2}\rangle$
$([532]\frac{3}{2}^-)$					$\|21\rangle$	$0.997\|5h_{11/2}\frac{11}{2}\rangle$
					$\|22\rangle$	$0.764\|5f_{7/2}\frac{1}{2}\rangle + 0.475\|5p_{3/2}\frac{1}{2}\rangle + 0.321\|5h_{9/2}\frac{1}{2}\rangle$
					$\|19\rangle$	$0.681\|5h_{11/2}\frac{1}{2}\rangle + 0.449\|5f_{5/2}\frac{1}{2}\rangle - 0.352\|5f_{7/2}\frac{1}{2}\rangle$
					$\|20\rangle$	$0.976\|5h_{9/2}\frac{9}{2}\rangle + 0.121\|5h_{9/2}\frac{5}{2}\rangle$
Band 3	−0.162	−0.164	0	15	$\|21\rangle$	$0.770\|5h_{9/2}\frac{9}{2}\rangle + 0.332\|5f_{7/2}\frac{7}{2}\rangle - 0.182\|5h_{9/2}\frac{3}{2}\rangle$
$([505]\frac{9}{2}^-)$					$\|22\rangle$	$0.815\|5h_{9/2}\frac{5}{2}\rangle + 0.394\|5h_{9/2}\frac{1}{2}\rangle - 0.221\|5f_{5/2}\frac{5}{2}\rangle$
					$\|23\rangle$	$0.752\|5h_{9/2}\frac{3}{2}\rangle - 0.392\|5h_{9/2}\frac{1}{2}\rangle - 0.372\|5h_{9/2}\frac{5}{2}\rangle$
					$\|19\rangle$	$0.998\|4g_{9/2}\frac{7}{2}\rangle$
					$\|20\rangle$	$0.935\|4d_{5/2}\frac{5}{2}\rangle + 0.235\|4g_{7/2}\frac{5}{2}\rangle + 0.151\|4g_{9/2}\frac{5}{2}\rangle$
Band 6	0.267	0.268	0	0	$\|21\rangle$	$0.941\|6i_{13/2}\frac{1}{2}\rangle + 0.337\|6g_{9/2}\frac{1}{2}\rangle$
$([660]\frac{1}{2}^+)$					$\|22\rangle$	$0.952\|6i_{13/2}\frac{3}{2}\rangle + 0.298\|6g_{9/2}\frac{3}{2}\rangle$
					$\|23\rangle$	$0.921\|4d_{3/2}\frac{3}{2}\rangle + 0.238\|4s_{1/2}\frac{1}{2}\rangle + 0.208\|5d_{5/2}\frac{3}{2}\rangle$

TABLE III. Same as Table I, but for ^{187}Tl.

Band	β		γ		$\|\nu\rangle$	Wave function in terms of $\|Nlj\Omega\rangle$
	Initial value	Fitted value	Initial value	Fitted value		
					$\|18\rangle$	$0.997\|5h_{11/2}\frac{9}{2}\rangle$
					$\|19\rangle$	$0.849\|5h_{9/2}\frac{1}{2}\rangle + 0.429\|5f_{5/2}\frac{1}{2}\rangle - 0.169\|5f_{7/2}\frac{1}{2}\rangle$
Band 1	0.250	0.253	0	0	$\|20\rangle$	$0.909\|5h_{9/2}\frac{3}{2}\rangle + 0.325\|5f_{5/2}\frac{1}{2}\rangle + 0.191\|5f_{7/2}\frac{3}{2}\rangle$
($[530]\frac{1}{2}^-$)					$\|21\rangle$	$1.000\|5h_{11/2}\frac{11}{2}\rangle$
					$\|22\rangle$	$0.741\|5f_{7/2}\frac{1}{2}\rangle + 0.480\|5p_{3/2}\frac{1}{2}\rangle + 0.327\|5h_{9/2}\frac{1}{2}\rangle$
					$\|18\rangle$	$0.997\|5h_{11/2}\frac{9}{2}\rangle$
					$\|19\rangle$	$0.868\|5h_{9/2}\frac{1}{2}\rangle + 0.410\|5f_{5/2}\frac{1}{2}\rangle - 0.162\|5f_{7/2}\frac{1}{2}\rangle$
Band 2	0.234	0.237	0	0	$\|20\rangle$	$0.916\|5h_{9/2}\frac{3}{2}\rangle + 0.312\|5f_{5/2}\frac{3}{2}\rangle + 0.189\|5f_{7/2}\frac{3}{2}\rangle$
($[532]\frac{3}{2}^-$)					$\|21\rangle$	$1.000\|5h_{11/2}\frac{11}{2}\rangle$
					$\|22\rangle$	$0.766\|5f_{7/2}\frac{1}{2}\rangle + 0.469\|5p_{3/2}\frac{1}{2}\rangle + 0.300\|5h_{9/2}\frac{1}{2}\rangle$
					$\|19\rangle$	$0.695\|5h_{11/2}\frac{1}{2}\rangle + 0.447\|5f_{5/2}\frac{1}{2}\rangle - 0.360\|5f_{7/2}\frac{1}{2}\rangle$
					$\|20\rangle$	$0.986\|5h_{9/2}\frac{9}{2}\rangle - 0.101\|5h_{9/2}\frac{5}{2}\rangle$
Band 3	-0.162	-0.162	0	15°	$\|21\rangle$	$0.780\|5h_{9/2}\frac{9}{2}\rangle + 0.348\|5f_{7/2}\frac{7}{2}\rangle - 0.169\|5h_{9/2}\frac{3}{2}\rangle$
($[505]\frac{9}{2}^-$)					$\|22\rangle$	$0.825\|5h_{9/2}\frac{5}{2}\rangle + 0.382\|5h_{9/2}\frac{1}{2}\rangle - 0.201\|5f_{5/2}\frac{5}{2}\rangle$
					$\|23\rangle$	$0.741\|5h_{9/2}\frac{3}{2}\rangle - 0.386\|5h_{9/2}\frac{1}{2}\rangle - 0.384\|5h_{9/2}\frac{5}{2}\rangle$
					$\|23\rangle$	$0.997\|6i_{13/2}\frac{13}{2}\rangle$
					$\|24\rangle$	$0.991\|6i_{13/2}\frac{11}{2}\rangle$
Band 5	-0.189	-0.192	0	11.3°	$\|25\rangle$	$0.974\|6i_{13/2}\frac{9}{2}\rangle$
($[606]\frac{13}{2}^+$)					$\|26\rangle$	$0.931\|6i_{13/2}\frac{7}{2}\rangle + 0.298\|6i_{13/2}\frac{3}{2}\rangle$
					$\|27\rangle$	$0.805\|6i_{13/2}\frac{5}{2}\rangle + 0.471\|6i_{13/2}\frac{1}{2}\rangle + 0.219\|5i_{13/2}\frac{3}{2}\rangle$
					$\|19\rangle$	$0.995\|4g_{7/2}\frac{7}{2}\rangle$
					$\|20\rangle$	$0.967\|4d_{5/2}\frac{5}{2}\rangle + 0.217\|4g_{7/2}\frac{5}{2}\rangle + 0.131\|4g_{9/2}\frac{5}{2}\rangle$
Band 6	0.267	0.265	0	0	$\|21\rangle$	$0.935\|6i_{13/2}\frac{1}{2}\rangle + 0.334\|6g_{9/2}\frac{1}{2}\rangle$
($[660]\frac{1}{2}^+$)					$\|22\rangle$	$0.946\|6i_{13/2}\frac{3}{2}\rangle + 0.303\|6g_{9/2}\frac{3}{2}\rangle$
					$\|23\rangle$	$0.906\|4d_{3/2}\frac{3}{2}\rangle + 0.245\|4s_{1/2}\frac{1}{2}\rangle + 0.214\|5d_{5/2}\frac{3}{2}\rangle$

$\chi^2 = \frac{1}{N}\sum_j (E_j^{\rm cal} - E_j^{\rm exp})^2$ of the energy spectrum of band 3 in ^{187}Tl (where N is the number of levels in the band) with respect to the value of γ at several β's in the upper panel of Fig. 2. We also display the variation of the calculated energy spectrum against the value of γ at the best fitted $\beta(-0.162)$ and the comparison with experimental data of the band in the lower panel of Fig. 2. The upper panel of Fig. 2 shows that the variation of the axial deformation parameter β (except for that with the angular deformation parameter γ in a special region) does not affect the calculation error χ^2 as drastically as that of the γ does. Combining the upper and the lower panels of Fig. 2, one can notice clearly that for zero γ, the calculation error χ^2 is quite large (about 60) and the calculated level sequence is not consistent with experiments. As γ increases to 3–5°, the calculated level sequence becomes consistent with the experimental one and χ^2 decreases to about 10^{-1}. For γ in the region of 3°–14°, χ^2 stays around 10^{-1}. When $\gamma = 15°$, χ^2 with $\beta = -0.162$ becomes suddenly the minimum ($\sim 10^{-4}$) of the $\chi^2(\beta, \gamma)$, and the calculated energy spectrum agrees with experimental data very well. As γ increases beyond 15°, χ^2 increases to around 10^{-3} and even to 10^{-1}. Moreover, in the case of $\beta = -0.162$, even though the calculated energies of the states with lower angular

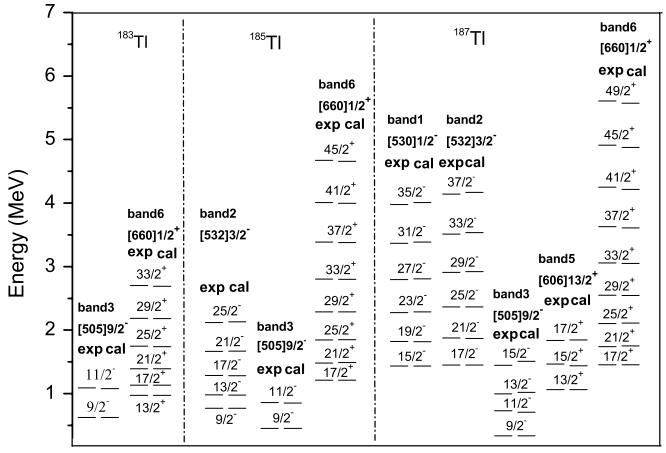

FIG. 1. Comparison of calculated energy levels of rotational bands in ^{183,185,187}Tl with experimental data from Refs. [6,8].

TABLE IV. Theoretically predicted main components of the wave functions of bands 1, 2, 3, 5 and 6 in ^{187}Tl in terms of the single-particle levels.

Band	I^π	Wave function $\|\nu K\rangle$
	$\frac{15}{2}^-$	$-0.981\|22\frac{1}{2}\rangle + 0.189\|19\frac{1}{2}\rangle$
	$\frac{19}{2}^-$	$0.981\|22\frac{1}{2}\rangle + 0.190\|19\frac{1}{2}\rangle$
Band 1	$\frac{23}{2}^-$	$0.980\|22\frac{1}{2}\rangle + 0.192\|19\frac{1}{2}\rangle$
$([530]\frac{1}{2}^-)$	$\frac{27}{2}^-$	$-0.980\|22\frac{1}{2}\rangle + 0.194\|19\frac{1}{2}\rangle$
	$\frac{31}{2}^-$	$0.979\|22\frac{1}{2}\rangle - 0.196\|19\frac{1}{2}\rangle$
	$\frac{35}{2}^-$	$0.979\|22\frac{1}{2}\rangle - 0.197\|19\frac{1}{2}\rangle$
	$\frac{17}{2}^-$	$-0.964\|20\frac{3}{2}\rangle + 0.263\|19\frac{1}{2}\rangle$
	$\frac{21}{2}^-$	$0.955\|20\frac{3}{2}\rangle - 0.294\|19\frac{1}{2}\rangle$
Band 2	$\frac{25}{2}^-$	$0.947\|20\frac{3}{2}\rangle - 0.321\|19\frac{1}{2}\rangle$
$([532]\frac{3}{2}^-)$	$\frac{29}{2}^-$	$-0.939\|20\frac{3}{2}\rangle + 0.343\|19\frac{1}{2}\rangle$
	$\frac{33}{2}^-$	$-0.932\|20\frac{3}{2}\rangle + 0.362\|19\frac{1}{2}\rangle$
	$\frac{37}{2}^-$	$-0.925\|20\frac{3}{2}\rangle + 0.378\|19\frac{1}{2}\rangle$
	$\frac{9}{2}^-$	$0.815\|20\frac{9}{2}\rangle + 0.444\|21\frac{7}{2}\rangle + 0.231\|23\frac{5}{2}\rangle$
Band 3	$\frac{11}{2}^-$	$0.728\|20\frac{9}{2}\rangle + 0.518\|21\frac{7}{2}\rangle - 0.299\|23\frac{5}{2}\rangle$
$([505]\frac{9}{2}^-)$	$\frac{13}{2}^-$	$0.500\|20\frac{9}{2}\rangle + 0.479\|21\frac{7}{2}\rangle + 0.399\|23\frac{5}{2}\rangle$
	$\frac{15}{2}^-$	$-0.584\|20\frac{9}{2}\rangle + 0.544\|21\frac{7}{2}\rangle - 0.388\|23\frac{5}{2}\rangle$
Band 5	$\frac{13}{2}^+$	$0.720\|23\frac{13}{2}\rangle + 0.520\|24\frac{11}{2}\rangle + 0.350\|25\frac{9}{2}\rangle$
$([606]\frac{13}{2}^+)$	$\frac{15}{2}^+$	$0.578\|23\frac{13}{2}\rangle - 0.560\|24\frac{11}{2}\rangle + 0.450\|25\frac{9}{2}\rangle$
	$\frac{17}{2}^+$	$-0.620\|23\frac{13}{2}\rangle - 0.390\|27\frac{5}{2}\rangle + 0.390\|26\frac{7}{2}\rangle$
	$\frac{17}{2}^+$	$-0.952\|21\frac{1}{2}\rangle - 0.298\|22\frac{3}{2}\rangle$
	$\frac{21}{2}^+$	$-0.943\|21\frac{1}{2}\rangle - 0.326\|22\frac{3}{2}\rangle$
Band 6	$\frac{25}{2}^+$	$0.936\|21\frac{1}{2}\rangle + 0.347\|22\frac{3}{2}\rangle$
$([660]\frac{1}{2}^+)$	$\frac{29}{2}^+$	$0.930\|21\frac{1}{2}\rangle + 0.363\|22\frac{3}{2}\rangle$
	$\frac{33}{2}^+$	$-0.924\|21\frac{1}{2}\rangle - 0.377\|22\frac{3}{2}\rangle$
	$\frac{37}{2}^+$	$0.919\|21\frac{1}{2}\rangle + 0.388\|22\frac{3}{2}\rangle$
	$\frac{41}{2}$	$0.915\|21\frac{1}{2}\rangle + 0.398\|22\frac{3}{2}\rangle$

momentum do not obviously deviate from experimental data, the ones with higher angular momentum do so drastically. It is then evident that, when the deformation parameters $(\beta, \gamma) = (-0.162, 15^\circ)$, the calculated energy spectrum agrees best with experimental data. It indicates that band 3 of ^{187}Tl is in triaxial oblate deformation. In addition, from Table IV, we notice that band 3 in ^{187}Tl comes mainly from the 20th single-particle orbital. As can be seen from inspecting Table III, the 20th orbital contains 97.2% $|5h_{9/2}\frac{9}{2}\rangle$ configuration. Therefore, band 3 can be identified as the one arising from the proton configuration $[505]\frac{9}{2}^-$ $(\pi\, h_{9/2})$ coupled to a triaxial oblate deformed core; this observation corroborates the conjecture in Ref. [6]. Similar results for bands 3 in ^{183,185}Tl are also obtained. The calculation error χ^2 of the energy separations against the value of γ at several β's and the comparison of the calculated energy spectrum with $\gamma \in (0^\circ, 29^\circ)$ and $\beta = -0.168$ (-0.164) with experimental data are illustrated in Fig. 3 (4) for ^{183}Tl (^{185}Tl). The deformation parameters can then be fixed as $(-0.168, 15^\circ)$ and $(-0.164, 15^\circ)$ for band 3 of ^{183}Tl and ^{185}Tl, respectively. These results confirm

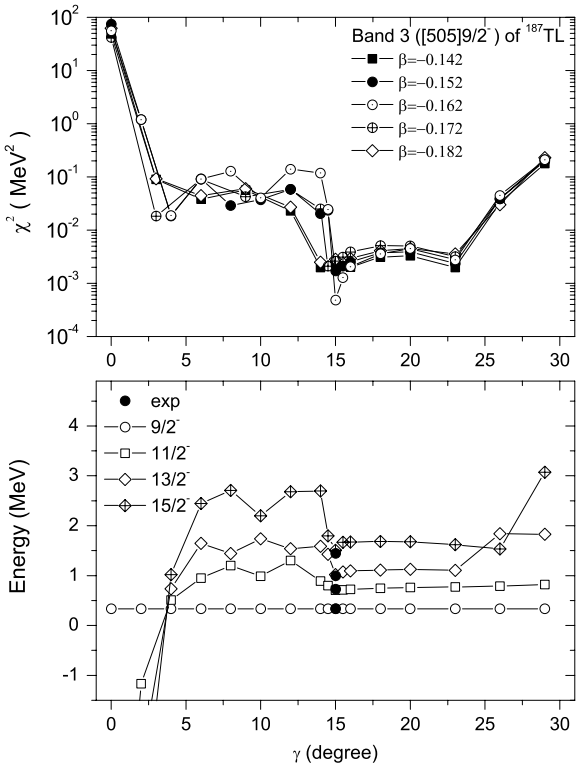

FIG. 2. Upper panel: calculation error χ^2 against the deformation parameter γ at several axial deformation parameter β's of band 3 in ^{187}Tl. Lower panel: variation of the calculated energy spectrum of band 3 in ^{187}Tl with fixed $\beta = -0.162$ against the value of γ and comparison with experimental data from Ref. [6].

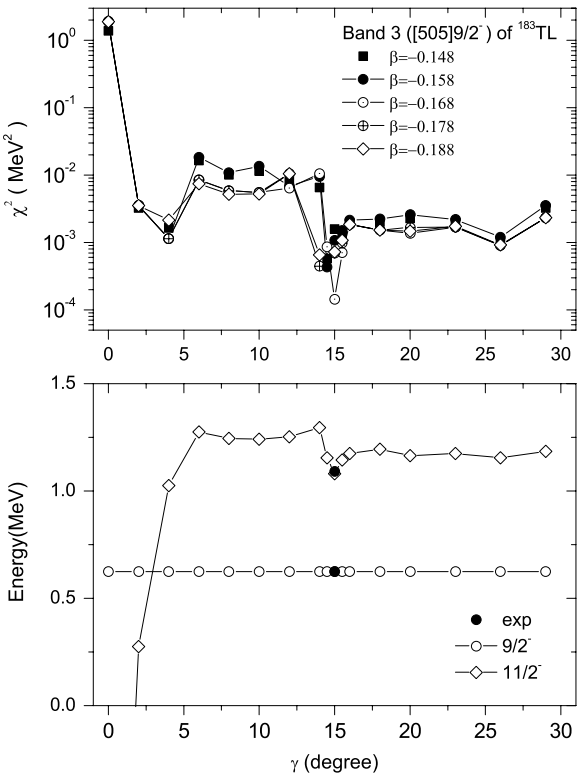

FIG. 3. Same as Fig. 2, but for ^{183}Tl and fixed $\beta = -0.168$. Experimental data are from Ref. [8].

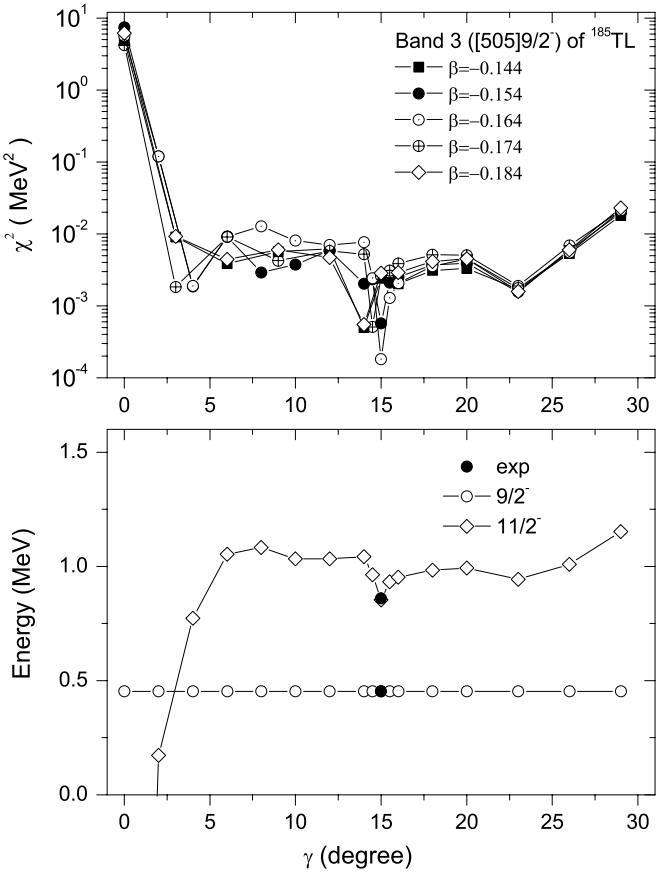

FIG. 4. Same as Fig. 2, but for ^{185}Tl and fixed $\beta = -0.164$. Experimental data are from Ref. [6].

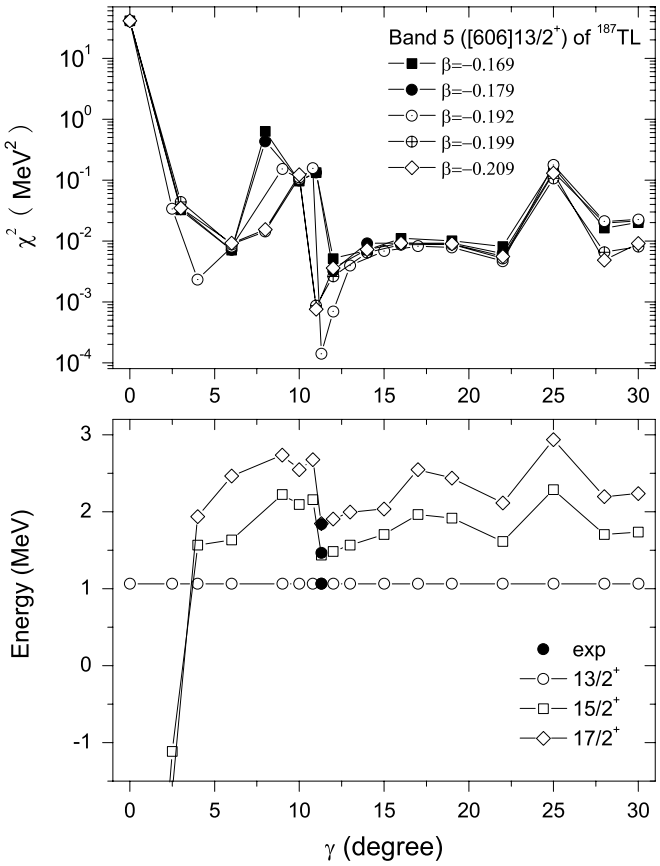

FIG. 5. Same as Fig. 2, but for band 5 in ^{187}Tl and fixed $\beta = -0.192$. Experimental data are from Ref. [6].

the assumption that the band that originated from orbital $[505]\frac{9}{2}^-$ ($\pi h_{9/2}$) may be in triaxial oblate deformation [6]. Besides, from the calculation error χ^2 and the comparison between the obtained energy spectrum with $\beta = -0.192$ and the experimental data of band $[606]\frac{13}{2}^+$ shown in Fig. 5, one can recognize that band 5 ($[606]\frac{13}{2}^+$ band) is also a triaxial oblate deformation band (with $(\beta, \gamma) = (-0.192, 11.3^\circ)$).

From the calculations, one may recognize that the deformation parameter γ influences the results more drastically than the axial deformation parameter β. By analyzing the obtained single-particle configuration, we know that the states in bands $[505]\frac{9}{2}^-$ and $[606]\frac{13}{2}^+$ involve much more complicated single-particle Nilsson configurations than the other bands. Such a result is consistent with that obtained for the nucleus ^{127}I in Ref. [20]. We infer then that the γ degree of freedom plays a more important role than β because it induces more obvious mixing among the single-particle Nilsson configurations.

IV. CONCLUSION AND REMARKS

In summary, we have systematically calculated the energy spectra, deformations, and wave functions of the rotational bands in nuclei ^{183,185,187}Tl in the particle-triaxial-rotor model with variable moment of inertia. The calculated energy spectra of the bands agree quite well with the experimental data. The configuration of the bands in ^{187}Tl is analyzed in detail as an example. We have also calculated the variation of the configuration of single-particle levels against the deformation parameters β and γ. Considering both the parameters fitted and the agreement between calculated results and experimental data, we conclude that the rotation-aligned band structures observed in ^{183,185,187}Tl are due to one of the $[530]\frac{1}{2}^-$, $[532]\frac{3}{2}^-$, $[660]\frac{1}{2}^+$ proton configurations coupled to a prolate deformed core. Furthermore, the negative parity bands built upon the $\frac{9}{2}^-$ isomeric states in ^{183,185,187}Tl are formed by a proton with the $[505]\frac{9}{2}^-$ configuration coupled to a core with triaxial oblate deformation $(\beta, \gamma) = (-0.168, 15^\circ)$, $(-0.164, 15^\circ)$, $(-0.162, 15^\circ)$, respectively; and the positive parity band on the $\frac{13}{2}^+$ isomeric state in ^{187}Tl is generated by a proton with configuration $[606]\frac{13}{2}^+$ coupled to a triaxial oblate core with deformation parameters $(\beta, \gamma) = (-0.192, 11.3^\circ)$. In short, the nuclei ^{183,185,187}Tl involve quite rich shape coexistence. In addition, our present calculation provides evidence that the triaxial deformation may arise from the mixing of single-particle Nilsson configurations. To understand that phenomenon better, more investigations are required.

ACKNOWLEDGMENTS

This work was partially supported by the Natural Science Foundation of Guangdong Province with Contract No. 04011642, the Natural Science Research Foundation of the Education Department of Guangdong Province with Contract No. Z02069, and the National Natural Science Foundation of China with Contract Nos. 10425521, 10135030, and 10075002. Y.X.L. thanks also the support given by the Major State Basic Research Development Program under Grant No. G2000077400, the Key Grant Project of Chinese Ministry of Education (CMOE) under Contract No. 305001, the Foundation for University Key Teacher by the CMOE, and the Research Fund for the Doctoral Programme of Higher Education of China with Grant No. 20040001010.

[1] K. Heyde, P. van Isacker, M. Waroquier, J. L. Wood, and R. A. Meyer, Phys. Rep. **102**, 291 (1983).
[2] J. L. Wood, K. Heyde, W. Nazarewicz, M. Huyse, and P. van Duppen, Phys. Rep. **215**, 101 (1992).
[3] R. M. Diamond and F. S. Stephens, Nucl. Phys. **45**, 632 (1963).
[4] J. O. Newton, S. D. Cirilov, F. S. Stephens, and R. M. Diamond, Nucl. Phys. **A148**, 593 (1970).
[5] J. A. Bounds, C. R. Bingham, P. Juncar, H. K. Carter, G. A. Leander, R. L. Mlekodaj, E. H. Spejewski, and W. M. Fairbank Jr., Phys. Rev. Lett. **55**, 2269 (1985).
[6] G. J. Lane, G. D. Dracoulis, A. P. Byrne, P. M. Walker, A. M. Baxter, J. A. Sheikh, and W. Nazarewicz, Nucl. Phys. **A586**, 316 (1995).
[7] W. Reviol, *et al*., Phys. Rev. C **61**, 044310 (2000).
[8] M. Muikku *et al*., Phys. Rev. C **64**, 044308 (2001).
[9] R. Bengtsson, T. Bengtsson, J. Dudek, G. Leander, W. Nazarewicz and J. Y. Zhang, Phys. Lett. **B183**, 1 (1987); R. Bengtsson and W. Nazarewicz, Z. Phys. A **334**, 269 (1989); R. Bengtsson, T. Bengtsson, M. Bergström, H. Ryde, and G. B. Hagemann, Nucl. Phys. **A569**, 469 (1994); R. Bengtsson, T. Bengtsson, and H. Ryde, Eur. Phys. J. A **22**, 355 (2004).
[10] F. R. Xu, P. M. Walker, J. A. Sheikh, and R. Wyss, Phys. Lett. **B435**, 257 (1998); F. R. Xu, W. Satuła, and R. Wyss, Nucl. Phys. **A669**, 119 (2000).
[11] V. I. Dimitrov, S. Frauendrof, and F. Dönau, Phys. Rev. Lett. **84**, 5732 (2000).
[12] K. Hara and Y. Sun, Int. J. Mod. Phys. E **4**, 637 (1995).
[13] J. Meyer-ter-Vehn, F. S. Stepens, and R. M. Diamond, Phys. Rev. Lett. **32**, 1383 (1974); J. Meyer-ter-Vehn, Nucl. Phys. **A249**, 111 (1975); **A249**, 141 (1975).
[14] S. E. Larsson, G. A. Leander, and I. Ragnarsson, Nucl. Phys. **A307**, 189 (1978).
[15] P. Ring and P. Schuck, *The Nuclear Many-Body Problem* (Springer-Verlag, New York, 1980).
[16] J. A. Sheikh and K. Hara, Phys. Rev. Lett. **82**, 3968 (1999); S. Frauendorf, K. Neergard, J. A. Sheikh, and P. M. Walker, Phys. Rev. C **61**, 064324 (2000); J. A. Sheikh, Y. Sun, and R. Palit, Phys. Lett. **B507**, 115 (2001).
[17] I. Hamamoto, Phys. Rev. C **65**, 044305 (2002).
[18] M. A. J. Mariscotti, G. Scharff-Goldhaber, and B. Buck, Phys. Rev. **178**, 1864 (1969).
[19] G. M. Zeng and H. C. Song, High Energy Phys. Nucl. Phys. (Chinese Edition) **26**, 1021 (2002).
[20] H. C. Song, Y. X. Liu, and Y. H. Zhang, Chin. Phys. Lett. **21**, 269 (2004).
[21] G. J. Chen, H. C. Song, and Y. X. Liu, Chin. Phys. Lett. **22**, 50 (2005).
[22] T. Bengtsson and I. Ragnarsson, Nucl. Phys. **A436**, 14 (1985).
[23] S. G. Nilsson and I. Ragnarsson, *Shapes and Shells in Nuclear Structure* (Cambridge University, Cambridge, England, 1995).